



## Experimental investigation and thermodynamic modelling of LiF-NdF<sub>3</sub>-DyF<sub>3</sub> system

A. Abbasalizadeh <sup>a,\*</sup>, S. Sridar <sup>b</sup>, Z. Chen <sup>a</sup>, M. Sluiter <sup>a</sup>, Y. Yang <sup>a</sup>, J. Sietsma <sup>a</sup>, S. Seetharaman <sup>c</sup>, K.C. Hari Kumar <sup>b</sup>

<sup>a</sup> Department of Materials Science & Engineering, Delft University of Technology, Delft, 2628 CD, The Netherlands

<sup>b</sup> Department of Metallurgical & Materials Engineering, Indian Institute of Technology Madras, Chennai, 600 036, India

<sup>c</sup> Royal Institute of Technology (KTH), Sweden

### ARTICLE INFO

#### Article history:

Received 20 November 2017

Received in revised form

1 March 2018

Accepted 2 April 2018

Available online 6 April 2018

#### Keywords:

Calphad  
LiF-DyF<sub>3</sub>  
DyF<sub>3</sub>-NdF<sub>3</sub>  
LiF-NdF<sub>3</sub>  
LiF-DyF<sub>3</sub>-NdF<sub>3</sub>  
DTA

### ABSTRACT

Electrolysis of molten fluorides is one of the promising methods for the recovery and recycling of rare earth metals from used magnets. Due to the dearth of phase equilibria data for molten fluoride systems, thermodynamic modelling of LiF-DyF<sub>3</sub>-NdF<sub>3</sub> system using the CALPHAD approach was carried out. Gibbs energy modelling for LiF-NdF<sub>3</sub> and LiF-DyF<sub>3</sub> systems was performed using the constitutional data from literature. *Ab initio* calculations were used to obtain enthalpy of reaction of LiDyF<sub>4</sub>, an intermediate phase that is found to exist in the LiF-DyF<sub>3</sub> system. Differential thermal analysis was carried out for selected compositions in the NdF<sub>3</sub>-DyF<sub>3</sub> system, in order to determine liquidus and solidus temperatures. The Gibbs energy parameters for the limiting binaries determined in this work is used for modelling the Gibbs energy functions of equilibrium phases in the ternary system. Selected compositions of LiF-NdF<sub>3</sub>-DyF<sub>3</sub> were subjected to DTA in order to validate the calculated phase temperatures involving melt.

© 2018 Elsevier B.V. All rights reserved.

## 1. Introduction

Rare earth elements are essential in the green and low-carbon economy due to their superior magnetic properties. They play a key role in hybrid and electric car industries as well as in wind turbines [1]. Neodymium along with dysprosium are expected to dominate the future of magnetic material industry, increasing their demand over the next 25 years by 700 and 2600%, respectively [2–4]. Due to the uneven distribution of the resources and recent issues in the supply and demand of the rare earth metals, demand for recovery of these metals from waste products is strongly rising. In comparison with the hydro metallurgical route, molten salt processes are advantageous due to the low energy consumption, higher purity of the end product, high efficiency and no limitation regarding the hydrogen evolution [5–7]. Molten salt electrolysis process is the dominant industrial method for extraction of rare earths [8]. Electrolysis of molten fluorides has been the subject of many studies on the recovery of rare earth metals [9–11]. Evolution of fluorine associated gases (PFCs), low solubility of the rare earth

oxide in the fluoride electrolytes and formation of oxyfluoride complexes are the challenges of the recovery of the rare earth elements.

In order to optimally design such processes, knowledge of phase equilibria and thermodynamics of molten fluorides system is crucial. However, there is a dearth of such information in the literature. In the present work, we report thermodynamic modelling of the LiF-DyF<sub>3</sub>-NdF<sub>3</sub> system using the CALPHAD approach.

## 2. Experiments

Anhydrous LiF (99.98%–Alfa Aesar, USA), DyF<sub>3</sub> (99.9%–Alfa Aesar, USA) and NdF<sub>3</sub> (99.9%–Alfa Aesar, USA) were used for preparing the samples for thermal analysis. Various compositions investigated in the NdF<sub>3</sub>-DyF<sub>3</sub> and LiF-DyF<sub>3</sub>-NdF<sub>3</sub> systems are listed in Tables 1 and 2, respectively. The samples were prepared by mixing the chemicals in a glove box and heating the mixture to a temperature above the melting point under Ar atmosphere and subsequently quenching the molten mixture using liquid nitrogen.

Differential thermal analysis (DTA) was carried out using Netzsch STA 409C apparatus with DTA/TG sample carrier. The instrument was calibrated by measuring the melting point of high

\* Corresponding author.

E-mail address: [A.Abbasalizadeh@tudelft.nl](mailto:A.Abbasalizadeh@tudelft.nl) (A. Abbasalizadeh).

**Table 1**Solidus and liquidus of NdF<sub>3</sub>-DyF<sub>3</sub> measured by DTA.

Composition (mol% DyF <sub>3</sub> )	Solidus	Liquidus
	(K)	
20	1569 (1603)	1646 (1640)
40	1519 (1491)	1606 (1612)
60	1449 (1444)	1549 (1560)
80	1418 (1429)	1492 (1465)

Values in parentheses are calculated.

purity metals such as Al, Ag, Au, Ni and Sn [12]. The signal related to temperature difference between the sample and the reference measured by DTA was converted into heat flux difference by means of an appropriate calibration. Hence the DTA results are reported as heat flux change with temperature. Each sample (weighing between 60 and 90 mg) was loaded in a platinum cup with a lid because of the corrosive character of fluoride salts. The platinum cup was positioned inside an alumina crucible. An empty alumina crucible served as the reference material. For each experiment, 3 cooling and heating runs were carried out. Heating rate was fixed at 10 K min<sup>-1</sup>, based on the instability of the fluoride salts. All experiments were carried out under high purity nitrogen atmosphere with a flow rate of 40 ml min<sup>-1</sup>.

### 3. Experimental results

#### 3.1. Thermal analysis

The extrapolated onset temperature is less affected by heating rate and other experimental factors in comparison with trough of the peak or offset temperature [13]. Hence, the DTA peaks were analysed using the onset technique reported by Ref. [14] in order to determine the phase transformation temperatures. Liquidus and solidus temperatures thus calculated from the heating and cooling curves, respectively, have an uncertainty of  $\pm 8$  K. The uncertainty is high due to the instability of the fluoride system and the difference between the second and third heating/cooling cycles.

DTA curves of NdF<sub>3</sub>-DyF<sub>3</sub> samples (Fig. 1 (a)) do not show any solid state transformation, which could be due to the small enthalpy of the orthorhombic to hexagonal transformation in DyF<sub>3</sub> [15]. The results from DTA analysis for the NdF<sub>3</sub>-DyF<sub>3</sub> mixtures indicate complete solubility of NdF<sub>3</sub> and DyF<sub>3</sub> and no evidence for any solid state phase transformation. All samples show only one peak in the heating curve corresponding to the solidus. Results are given in Table 1. The maximum weight loss of the samples measured by thermogravimetric analysis (TGA), was 1.43%.

The phase transformation temperature for the LiF-DyF<sub>3</sub>-NdF<sub>3</sub> system was also obtained using the DTA. In Fig. 1(b), the DTA curves corresponding to LiF-30 mol% NdF<sub>3</sub>-30 mol% DyF<sub>3</sub> composition show two peaks. The transformation temperatures are measured to be 955 and 1053 K, respectively. Except for LiF-30 mol% NdF<sub>3</sub>-30 mol% DyF<sub>3</sub>, all DTA results for the ternary compositions show one

peak while three thermal events are expected for each composition. High heating rate and mass loss in the samples can be two reasons that these transitions are not captured by DTA. Because of the high evaporation of salts, especially LiF, which results in the mass loss of the samples, reliable measurement of the transformation temperatures of LiF-DyF<sub>3</sub>-NdF<sub>3</sub> system using DTA is difficult. The mass loss of the samples increased with the increase in the amount of LiF in the samples. For the sample LiF-10 mol% NdF<sub>3</sub>-10 mol% DyF<sub>3</sub>, the mass loss was measured to be about 34%. Moreover, in ternary systems some of the compositions go through four-phase as well as three-phase regions in addition to the two-phase region before melting is completed. Some of these events are not necessarily captured in a DTA experiment. Hence, the DTA results were only used for comparing with the calculated results. The phase transformation temperatures determined by DTA for all ternary compositions are listed in Table 2.

#### 3.2. Microstructure analysis

In order to investigate the solubility of the solid phase at high temperatures in the NdF<sub>3</sub>-DyF<sub>3</sub> system, the samples were heated below the liquidus temperature and quenched in liquid nitrogen. The quenched samples were subjected to SEM/EDS to ascertain the number of phases present at various compositions of NdF<sub>3</sub>-DyF<sub>3</sub>. The results (Fig. 2) show the presence of a single phase in all investigated samples, proving extended solid solubility just below their solidus. No evidence of phase separation could be detected in any of the samples.

### 4. Ab initio calculations

Due to lack of experimental thermochemical information for the compound LiDyF<sub>4</sub> forming in LiF-DyF<sub>3</sub> system, *ab initio* calculations were performed to estimate its enthalpy of formation. The Vienna *Ab initio* Simulation Package (VASP) [16,17] was used. The input parameters used for relaxing the structures are listed in Table 3. The enthalpies of formation of LiDyF<sub>4</sub> in tetragonal (I4<sub>1</sub>/a) and orthorhombic (Pb24, Pbcn) structures were estimated. It was found that tetragonal LiDyF<sub>4</sub> was more stable in comparison with the orthorhombic LiDyF<sub>4</sub>.

The enthalpy of the reaction  $\text{LiF} + \text{DyF}_3 \rightleftharpoons \text{LiDyF}_4$  was calculated according to Equation (1).

$$\Delta_f H_{298}^{\circ}(\text{LiDyF}_4) \approx E_0(\text{LiDyF}_4) - E_0(\text{LiF}) - E_0(\text{DyF}_3) \quad (1)$$

In order to validate the calculated  $\Delta_f H_{298}^{\circ}$  for LiDyF<sub>4</sub>, the enthalpies of formation of LiF and DyF<sub>3</sub> were also calculated with the same input parameters as in Table 3 using VASP. The  $\Delta_f H_{298}^{\circ}$  for these compounds were calculated using Equation (2).

$$\Delta_f H_{298}^{\circ}(\text{AF}_y) \approx E_0(\text{AF}_y) - E_0(\text{A}) - \frac{y}{2}E_0(\text{F}_2) \quad (2)$$

The enthalpy of formation of LiF was calculated with respect to Li(bcc) and F<sub>2</sub>(gas) and DyF<sub>3</sub> was calculated with respect to Dy(dhcp) and F<sub>2</sub>(gas). The total energy of F<sub>2</sub>(gas) was calculated using the same procedure as in Ref. [21] for calculating the total energy of N<sub>2</sub>(gas). The difference in total energies of DyF<sub>3</sub> with hexagonal (P<sub>3</sub>c1) and orthorhombic (Pnma) structures was also calculated. The calculated enthalpies from the present work and the comparison with experimental data from literature are listed in Table 4.

### 5. Thermodynamic models

There are five equilibrium phases in this system: Liquid, Cubic

**Table 2**Phase transformation temperatures of LiF-NdF<sub>3</sub>-DyF<sub>3</sub> measured by DTA.

Composition (mol% DyF <sub>3</sub> )	(mol% LiF)	Temperature
		(K)
10	80	982 (981, L+Cub ⇌ L+Cub+Hex)
20	60	948 (955, L ⇌ Cub+Hex+LiDyF <sub>4</sub> )
40	40	1063 (1063, L+Hex ⇌ L+Hex+LiDyF <sub>4</sub> )
30	40	1053 (1045, L+Hex ⇌ L+Hex+LiDyF <sub>4</sub> )
20	20	1038 (1037, L+Hex ⇌ L+Hex+LiDyF <sub>4</sub> )

Values in parentheses are calculated. Corresponding phase transformations are also given.

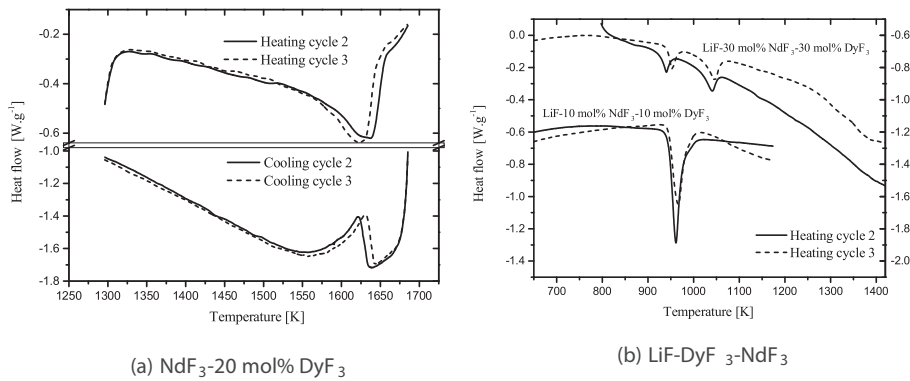


Fig. 1. DTA thermograms of representative compositions.

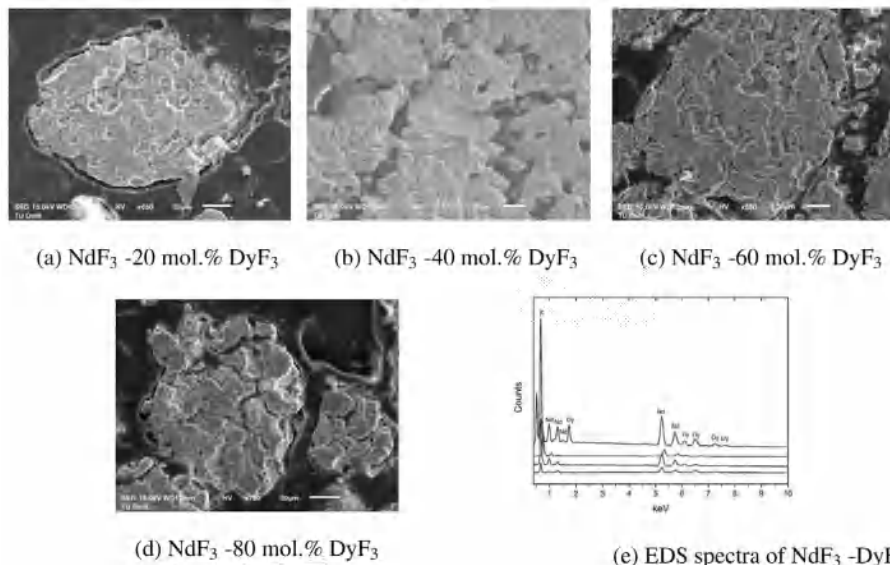


Fig. 2. BSE images and EDS spectra of selected compositions.

(Cub), Orthorhombic (Ort), Hexagonal (Hex) and LiDyF<sub>4</sub>. The crystallographic information for the solid phases of the system is listed in Table 5.

The liquid phase was modelled using the two-sublattice model for ionic melts [25,26]. This is based on Temkin's model [27] assuming that cations and anions occupy separate sublattices (indicated by parenthesis in Table 6) and mix randomly within each sublattice. The mixing model for liquid phase is thus represented as

$$(Dy^{3+}, Li^+, Nd^{3+})_p : (F^-, LiDyF_4)_q$$

**Table 3**  
VASP input parameters.

Potential	PAW [18]
Exchange-correlation functional	GGA-PBE [19]
Energy cut-off	600 eV
k-point mesh spacing	$\leq 0.8 \text{ \AA}^{-1}$
Force convergence	$1 \times 10^{-3} \text{ eV/\AA}$
Stress convergence	0.1 kB
SCF convergence	$1 \times 10^{-4} \text{ eV}$
Integration scheme	Tetrahedron method with Blöchl correction [20]

Initially, the liquid phase was modelled without a neutral species in the anion sublattice. It was found that several model parameters were required to obtain the best-fit to experimental data. Hence, LiDyF<sub>4</sub> (corresponding to the stoichiometry of the most stable compound in the system) was added as a fictitious neutral species to account for the short range ordering in LiF-DyF<sub>3</sub> melt. In order to keep the electroneutrality, the number of sites on each sublattice, *p* and *q*, must satisfy the following constraints:

$$p = y_{F^-} \quad (3)$$

$$q = 3y_{Dy^{3+}} + y_{Li^+} + 3y_{Nd^{3+}} \quad (4)$$

**Table 4**  
Enthalpies of reaction/formation of LiDyF<sub>4</sub>, LiF and DyF<sub>3</sub>.

Phase	$\Delta_f H_{298}^\circ / \Delta_f H_{298}^\circ$ (kJ/mol)	Experiment
	Ab initio	
LiDyF <sub>4</sub>	-19.156	-
LiF	-574.626	-594.581[22]
DyF <sub>3</sub>	-1606.664	-1665.23[23]
		-1692[24]

**Table 5**  
Crystallographic data for solid phases.

Phase	Space group	Stability range (K)
Cub (LiF)	Fm $\bar{3}$ m	$\leq 1121$
Ort (DyF <sub>3</sub> )	Pnma	$\leq 1300$
Hex (DyF <sub>3</sub> )	P6 <sub>3</sub> /mmc	1300 – 1430
Hex (NdF <sub>3</sub> )	P6 <sub>3</sub> /mmc	$\leq 1650$
LiDyF <sub>4</sub>	I4 <sub>1</sub> /a	$\leq 1093$

**Table 6**  
Sublattice formulations for the phases.

Phase	Sublattice formulation
Liquid	(Dy <sup>3+</sup> , Li <sup>+</sup> , Nd <sup>3+</sup> ) <sub>p</sub> : (F <sup>-</sup> , LiDyF <sub>4</sub> ) <sub>q</sub>
Cub	(Li <sup>+</sup> ) <sub>1</sub> : (F <sup>-</sup> ) <sub>1</sub>
Hex	(Dy <sup>3+</sup> , Nd <sup>3+</sup> ) <sub>1</sub> : (F <sup>-</sup> ) <sub>3</sub>
Ort	(Dy <sup>3+</sup> ) <sub>1</sub> : (F <sup>-</sup> ) <sub>3</sub>
LiDyF <sub>4</sub>	(Dy <sup>3+</sup> ) <sub>1</sub> : (Li <sup>+</sup> ) <sub>1</sub> : (F <sup>-</sup> ) <sub>3</sub>

**Table 7**  
Data sources used for the optimization.

Data	Method	Reference
LiF-NdF <sub>3</sub>		
Liquidus	DTA	[34]
LiF-DyF <sub>3</sub>		
Liquidus	DTA	[34]
$\Delta_i H_{298}^{\circ}$	DFT	Present work
NdF <sub>3</sub> -DyF <sub>3</sub>		
Liquidus/Solidus	DTA	Present work

Cubic, orthorhombic and LiDyF<sub>4</sub> phases were modelled as stoichiometric phases. Hexagonal phase was modelled as solid solution based on the compound energy formalism [28,29]. According to this approach, the structure of a phase is represented by two or more sublattices and constituent species mix randomly within the sublattices. Table 6 summarizes the sublattice formulations used in the Gibbs energy modelling of various phases. The Gibbs energy

expressions for LiF (cubic and liquid), NdF<sub>3</sub> (hexagonal and liquid) and DyF<sub>3</sub> (hexagonal and liquid) are from the SGTE substance database (Version 5.1) [30]. The Gibbs energy expression for DyF<sub>3</sub> (orthorhombic) is estimated using enthalpy and temperature DyF<sub>3</sub> (orthorhombic) to DyF<sub>3</sub> (hexagonal) transformation. This is explained in Section 7.1.

## 6. Optimization

The Gibbs energy parameter optimization was carried out using the PARROT module [31] of the Thermo-Calc data bank system [32] using relevant constitutional and thermochemical data as input. The method involves minimizing reduced sum of squares of errors in an iterative manner, starting with estimated values for all optimizing variables. Optimized Gibbs energy description thus obtained, is eventually used for calculating phase diagrams and thermochemical properties at any desired temperature and composition regime in which the functions are valid. The sources of input data used in the optimization are shown in Table 7. Optimization is initialized by providing estimated values for the parameters. The start values are refined iteratively by minimizing the sum of the squares of deviation between input data and the corresponding model calculated values. Finally the model parameters were rounded-off according to the method suggested by Hari Kumar et al. [33]. The Gibbs energy parameters of LiF-NdF<sub>3</sub>, LiF-DyF<sub>3</sub> and NdF<sub>3</sub>-DyF<sub>3</sub> were optimized based on this method. Optimization was not performed for the ternary system.

## 7. Results

### 7.1. Binary systems

The optimized thermodynamic parameters for LiF-NdF<sub>3</sub>, LiF-DyF<sub>3</sub> and DyF<sub>3</sub>-NdF<sub>3</sub> systems obtained in this work are listed in Table 8.

The phase diagram of LiF-NdF<sub>3</sub> calculated using the model parameters obtained in this work is shown in Fig. 3 along with the experimental data from Ref. [34]. The phase diagram of LiF-NdF<sub>3</sub> is a simple eutectic phase diagram without any solid solubility in

**Table 8**  
Gibbs energy parameters for DyF<sub>3</sub>-LiF-NdF<sub>3</sub> system (in SI units).

$$\text{GHSERDF} = -1722267.41 + 512.670134T - 92.91541T \ln(T) - 0.01096079T^2 - 2.12147 \times 10^{-10}T^3 + 235586.75T^{-1} \quad (298.15 < T < 1430) - 1791020.92 + 1010.0659T - 156.97 \ln(T) \quad (1430 < T < 6000)$$

$$\text{GHSERLF} = -634621.638 + 305.645567T - 50.306327 \ln(T) + 0.0012289475T^2 - 2.30170167 \times 10^{-6}T^3 + 399408.87T^{-1} \quad (298.15 < T < 700) - 633813.702 + 278.759762T - 45.752467 \ln(T) - 0.0060330357T^2 - 4.40324167 \times 10^{-7}T^3 + 433813.85T^{-1} \quad (700 < T < 1121) - 644878.626 + 411.074928T - 64.182567 \ln(T) \quad (1121 < T < 3000)$$

$$\text{GHSERNF} = -1710301.85 + 510.665061T - 92.69601T \ln(T) - 0.01171485T^2 - 1.08333333 \times 10^{-10}T^3 + 322770T^{-1} \quad (298.15 < T < 1650) - 1809836.14 + 1142.45411T - 172.4*T \ln(T) - 1.1335 \times 10^{-4}T^2 \quad (1650 < T < 6000)$$

$$\text{Liquid: } (\text{Dy}^{3+}, \text{Li}^+, \text{Nd}^{3+})_p : (\text{F}^-, \text{LiDyF}_4)_q \quad G_{\text{Dy}^{3+}, \text{F}^-}^{\text{Liquid}} = +\text{GHSERDF} + 58576 - 40.9622387T \quad G_{\text{Li}^+, \text{F}^-}^{\text{Liquid}} = +\text{GHSERLF} + 27087.2 - 24.1569607T \quad G_{\text{Nd}^{3+}, \text{F}^-}^{\text{Liquid}} = +\text{GHSERNF} + 54810 - 33.2181818T \quad G_{\text{LiDyF}_4}^{\text{Liquid}} = \text{GHSERLF} + \text{GHSERDF} + 85663.2 - 65.1191994T \quad L_{\text{Dy}^{3+}, \text{Li}^+, \text{F}^-}^{\text{Liquid}} = -46814^1L_{\text{Dy}^{3+}, \text{Li}^+, \text{F}^-}^{\text{Liquid}} = +10509^2L_{\text{Dy}^{3+}, \text{Li}^+, \text{F}^-}^{\text{Liquid}} = +18849^0L_{\text{Li}^+, \text{Nd}^{3+}, \text{F}^-}^{\text{Liquid}} = +27447 - 41.475T^0L_{\text{Dy}^{3+}, \text{Nd}^{3+}, \text{F}^-}^{\text{Liquid}} = +9956^1L_{\text{Dy}^{3+}, \text{Nd}^{3+}, \text{F}^-}^{\text{Liquid}} = -3863^0L_{\text{Dy}^{3+}, \text{Li}^+, \text{F}^-, \text{LiDyF}_4}^{\text{Liquid}} = +178255$$

$$\text{Cub: } (\text{Li}^+)_1 : (\text{F}^-)_1 \quad G_{\text{Li}^+, \text{F}^-}^{\text{Cub}} = +\text{GHSERLF}$$

$$\text{Hex: } (\text{Dy}^{3+}, \text{Nd}^{3+})_1 : (\text{F}^-)_3 \quad G_{\text{Dy}^{3+}, \text{F}^-}^{\text{Hex}} = +\text{GHSERDF} \quad G_{\text{Nd}^{3+}, \text{F}^-}^{\text{Hex}} = +\text{GHSERNF}$$

$$0^1L_{\text{Dy}^{3+}, \text{Nd}^{3+}, \text{F}^-}^{\text{Hex}} = +10316^1L_{\text{Dy}^{3+}, \text{Nd}^{3+}, \text{F}^-}^{\text{Hex}} = +8164$$

$$\text{Ort: } (\text{Dy}^{3+})_1 : (\text{F}^-)_3 \quad G_{\text{Dy}^{3+}, \text{F}^-}^{\text{Ort}} = +\text{GHSERDF} - 13532 + 10.409T$$

$$\text{LiDyF}_4: (\text{Dy}^{3+})_1 : (\text{Li}^+)_1 : (\text{F}^-)_3 \quad G_{\text{Dy}^{3+}, \text{Li}^+, \text{F}^-}^{\text{LiDyF}_4} = +\text{GHSERDF} + \text{GHSERLF} - 51636 + 28.9T$$

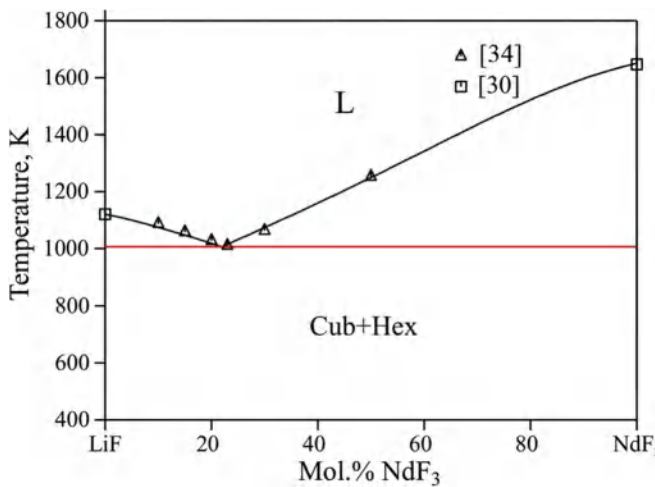


**Fig. 3.** Calculated LiF-NdF<sub>3</sub> phase diagram and its comparison with the experimental data from Ref. [34].

cubic and hexagonal phases. The optimized eutectic composition and temperature for this system are 22 mol% NdF<sub>3</sub> and 1007 K, respectively.

LiF-DyF<sub>3</sub> phase diagram was optimized using the experimental data by Thoma et al. [34] along with the enthalpy of reaction of LiDyF<sub>4</sub> obtained from *ab initio* calculation. The calculated phase diagram is shown in Fig. 4. Here also the terminal solid phases have no solubilities. The calculated enthalpy of reaction of LiDyF<sub>4</sub> ( $-19.052 \text{ kJ/mol}$ ) is in good agreement with the *ab initio* calculated value that was used as the input.

Zalkin and Tempelton [35] were the first to recognise the dimorphism among the rare earth trifluorides. They observed hexagonal structure for LaF<sub>3</sub> to NdF<sub>3</sub> and orthorhombic structure for GdF<sub>3</sub> to LuF<sub>3</sub>, while SmF<sub>3</sub>, EuF<sub>3</sub>, HoF<sub>3</sub> and TmF<sub>3</sub> could have both hexagonal and orthorhombic structure. Thoma and Brunton [23] also studied the dimorphism of lanthanide trifluorides systematically. They observed Tysonite-type hexagonal structure for LaF<sub>3</sub> to NdF<sub>3</sub> group. However, they have found that all lanthanide trifluorides with the orthorhombic structure transform to hexagonal crystal structure on heating. They have demonstrated that SmF<sub>3</sub>, EuF<sub>3</sub>, TbF<sub>3</sub> and DyF<sub>3</sub> form Tysonite-type hexagonal structure, while

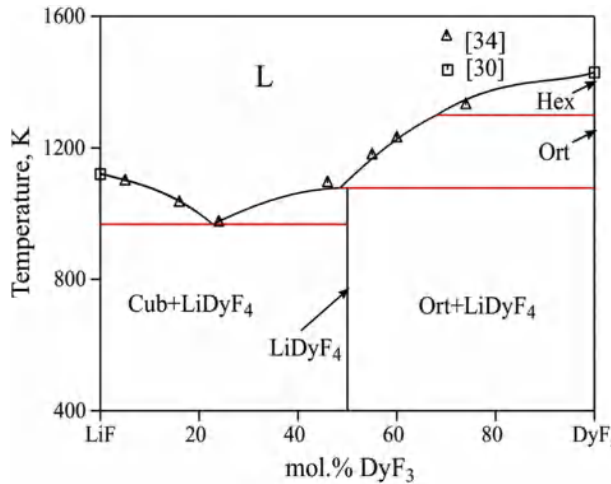


**Fig. 4.** Calculated LiF-DyF<sub>3</sub> phase diagram and its comparison with the experimental data from Ref. [34].

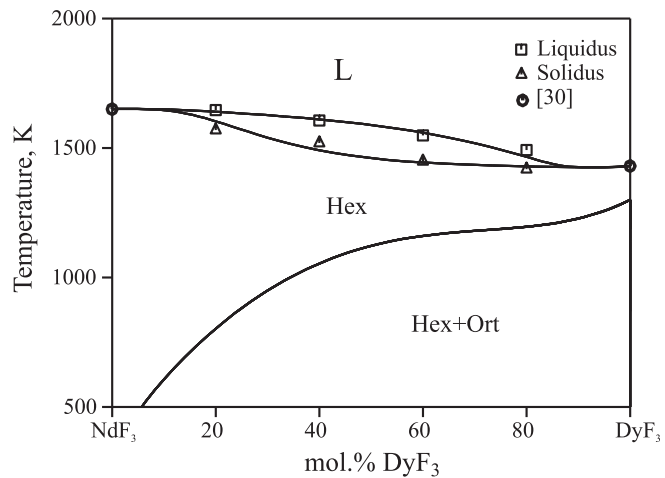


**Fig. 5.** Calculated NdF<sub>3</sub>-DyF<sub>3</sub> phase diagram and its comparison with the experimental data from present work.

ErF<sub>3</sub> to LuF<sub>3</sub> form  $\alpha$ -YF<sub>3</sub> type structure. Spedding et al. [36,37] confirmed the orthorhombic to hexagonal transformation for TbF<sub>3</sub> and DyF<sub>3</sub> by high temperature XRD. However, the enthalpy of the transformation for these two fluorides was not large enough to be detected by drop calorimetry. Greis and Cader [15] have not observed any first-order solid state transformation for TbF<sub>3</sub>, DyF<sub>3</sub> and HoF<sub>3</sub>.

Sobolev et al. found that presence of oxygen can influence the structure of lanthanide trifluoride, which can be a source of discrepancy [38,39]. Meanwhile, Garashina et al. [40] have observed that the transformation of orthorhombic to hexagonal structure takes place as a result of a deformational mechanism and over a broad temperature range. Stankus et al. [41] have proposed that orthorhombic to hexagonal transformation in lanthanide trifluorides proceeds in two stages: first a continuous transformation up to the transformation temperature ( $T_t$ ) and then a sharp change of lattice parameters at  $T_t$ .

The enthalpy of the orthorhombic to hexagonal transformation in DyF<sub>3</sub> was measured by drop calorimetry by Lyaponov et al. [42].

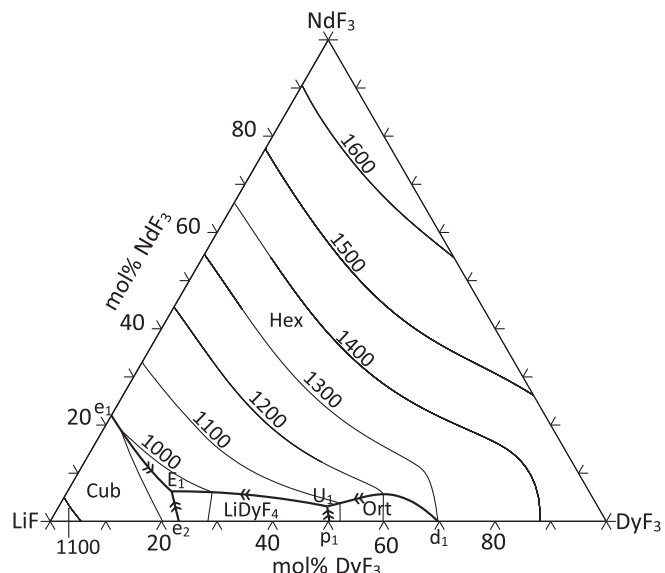


**Fig. 6.** Calculated liquidus projection.

**Table 9**  
Details of phase transformations in  $\text{LiF-NdF}_3\text{-DyF}_3$  system.

Transformation	Liquid composition (mol%)		Temperature (K)	Reference
	LiF	$\text{DyF}_3$		
<b>LiF-NdF<sub>3</sub></b>				
$\text{L} \rightleftharpoons \text{Cub}$	100	0	1121	[30]
$\text{L} \rightleftharpoons \text{Hex}$	0	0	1652	[30]
$\text{L} \rightleftharpoons \text{Cub} + \text{Hex} (\text{e}_1)$	78	0	1007	This work
	77	0	1011	[34]
	74.7	0	1006.5	[43]
<b>LiF-DyF<sub>3</sub></b>				
$\text{L} \rightleftharpoons \text{Hex}$	0	100	1430	[30]
$\text{L} \rightleftharpoons \text{Cub} + \text{LiDyF}_4 (\text{e}_2)$	77.2	22.8	968	This work
	76	24	973	[34]
$\text{L} + \text{Ort} \rightleftharpoons \text{LiDyF}_4 (\text{p}_1)$	51.4	48.6	1078	This work
	54	46	1093	[34]
$\text{L} + \text{Hex} + \text{Ort} (\text{d}_1)$	31.9	68.1	1300	This work
<b>DyF<sub>3</sub>-LiF-NdF<sub>3</sub></b>				
$\text{L} + \text{Ort} \rightleftharpoons \text{Hex} + \text{LiDyF}_4 (\text{U}_1)$	48.64	48.25	1068	This work
$\text{L} \rightleftharpoons \text{Hex} + \text{Cub} + \text{LiDyF}_4 (\text{E}_1)$	75.05	18.77	955	This work

They reported that the transformation takes place at 1300 K and the corresponding enthalpy change is  $+2400 \pm 1700 \text{ J mol}^{-1}$ . Since there is large uncertainty in the reported enthalpy value, we preferred using the corresponding DFT calculated value ( $+3383 \text{ J mol}^{-1}$ ) along with the measured temperature of transformation (1300 K) to describe the Gibbs energy of  $\text{DyF}_3$  (orthorhombic).

The solidus-liquidus data obtained by DTA in the current work were used for optimization of Gibbs energy model parameters in the  $\text{NdF}_3\text{-3DyF}_3$  system. The calculated phase diagram along with experimental data from the present work is shown in Fig. 5. The phase diagram shows extended solubility in the hexagonal phase in the high temperature region. As it was discussed earlier in this paper, both the DTA measurements and microstructure analysis indicated the complete solubility of  $\text{NdF}_3$  and  $\text{DyF}_3$ .

## 7.2. $\text{DyF}_3\text{-LiF-NdF}_3$

The liquidus projection along with the isotherms is shown in Fig. 6. It is calculated using the Gibbs energy parameters of binaries alone. No ternary parameters were used. The projection shows two ternary invariant transformations, whose co-ordinates are also

listed in Table 9. The corresponding Scheil reaction scheme is shown in Fig. 7. Table 2 gives a comparison of DTA results with calculated phase transformation temperatures and the corresponding phase changes.

## 8. Conclusions

The Gibbs energy parameters for  $\text{LiF-DyF}_3$  and  $\text{LiF-NdF}_3$  systems were optimized with experimental data from literature. *Ab initio* calculations were used to obtain the enthalpy of formation for  $\text{LiDyF}_4$ , which is a stable phase in the  $\text{LiF-DyF}_3$  system.  $\text{NdF}_3\text{-DyF}_3$  system optimization was performed with the experimental data obtained from DTA analysis in this work. The phase diagram of  $\text{DyF}_3\text{-LiF-NdF}_3$  system was computed based on the Gibbs parameters of the three limiting binaries and compared with the phase diagram data obtained by DTA experiments. All the calculated phase diagrams are in good agreement with the experimental data.

## References

- K. Binnemanns, P.T. Jones, B. Blanpain, T. Van Gerven, Y. Yang, A. Walton, M. Buchert, Recycling of rare earths: a critical review, *J. Clean. Prod.* 51 (0) (2013) 1–22.
- I. Rampin, F. Bisaglia, M. Dabalà, Corrosion properties of NdFeB Magnets Coated by a Ni/Cu/Ni layer in chloride and sulfide environments, *J. Mater. Eng. Perform.* 19 (7) (2010) 970–975.
- J. Coey, Permanent magnet applications, *J. Magn. Magn. Mater.* 248 (3) (2002) 441–456.
- E. Alonso, A.M. Sherman, T.J. Wallington, M.P. Everson, F.R. Field, R. Roth, R.E. Kirchain, Evaluating rare earth element availability: a case with revolutionary demand from clean technologies, *Environ. Sci. Technol.* 46 (6) (2012) 3406–3414.
- Y. Castrillejo, M.R. Bermejo, P. Díaz Arocás, A.M. Martínez, E. Barrado, Electrochemical behaviour of praseodymium (iii) in molten chlorides, *J. Electroanal. Chem.* 575 (1) (2005) 61–74.
- B. Mishra, D.L. Olson, Molten salt applications in materials processing, *J. Phys. Chem. Solid.* 66 (2–4) (2005) 396–401.
- W. Han, Q. Chen, Y. Sun, T. Jiang, M. Zhang, Electrodeposition of Mg-Li-Al-La alloys on inert cathode in molten LiCl-KCl eutectic salt, *Metall. Mater. Trans. B* 42 (6) (2011) 1367–1375.
- P. Siming, Y. Shihong, L. Zongan, C. Dehon, X. Liha, Z. Bin, Development on molten salt electrolytic methods and technology for preparing rare earth metals and alloys in China, *Chin. J. Rare Earth* 35 (3) (2011) 440–450.
- J. Lodermeyeier, M. Multerer, M. Zistler, S. Jordan, H.J. Gores, W. Kipferl, E. Diaconu, M. Sperl, G. Bayreuther, Electroplating of dysprosium, electrochemical investigations, and study of magnetic properties, *J. Electrochem. Soc.* 153 (4) (2006) 242–248.
- A. Abbasalizadeh, L. Teng, S. Sridhar, S. Seetharaman, Neodymium extraction using salt extraction process, *Miner. Process. Extr. Metall. (IMM Trans. Sect. C)* 124 (4) (2015) 191–198.
- A. Abbasalizadeh, A. Malfiet, S. Seetharaman, J. Sietsma, Y. Yang, Electrochemical extraction of rare earth metals in molten fluorides: conversion of rare earth oxides into rare earth fluorides using fluoride additives, *J. Sustain. Metall.* 3 (2017) 627–637.
- G. Höhne, H. Cammenga, W. Eysel, E. Gmelin, W. Hemminger, The temperature calibration of scanning calorimeters, *Thermochim. Acta* 160 (1) (1990) 1–12.
- M.I. Pope, Differential Thermal Analysis—a Guide to Technique and its Applications, Heyden, London, 1977.
- G. Lombardi, For Better thermal Analysis, Tech. rep., Confederation for Thermal Analysis, University of Rome, 1980.
- O. Greis, M. Cader, Polymorphism of high-purity rare earth trifluorides, *Thermochim. Acta* 87 (1985) 145–150.
- G. Kresse, J. Furthmüller, Efficient iterative schemes for ab initio total-energy calculations using a plane-wave basis set, *Phys. Rev. B Condens. Matter* 54 (16) (1996) 11169–11186.
- G. Kresse, J. Furthmüller, Efficiency of ab-initio total energy calculations for metals and semiconductors using a plane-wave basis set, *Comput. Mater. Sci.* 6 (1) (1996) 15–50.
- P.E. Blöchl, Projector augmented-wave method, *Phys. Rev. B* 50 (24) (1994) 17953.
- J.P. Perdew, K. Burke, M. Ernzerhof, Generalized gradient approximation made simple, *Phys. Rev. Lett.* 77 (1996) 3865.
- P.E. Blöchl, O. Jepsen, O.K. Andersen, Improved tetrahedron method for Brillouin-zone integrations, *Phys. Rev. B* 49 (1994) 16223.
- A. Zoroddu, F. Bernardini, P. Ruggerone, V. Fiorentini, First-principles prediction of structure, energetics, formation enthalpy, elastic constants, polarization, and piezoelectric constants of AlN, GaN, and InN: comparison of local and gradient-corrected density-functional theory, *Phys. Rev. B* 64 (2001), 1–10.

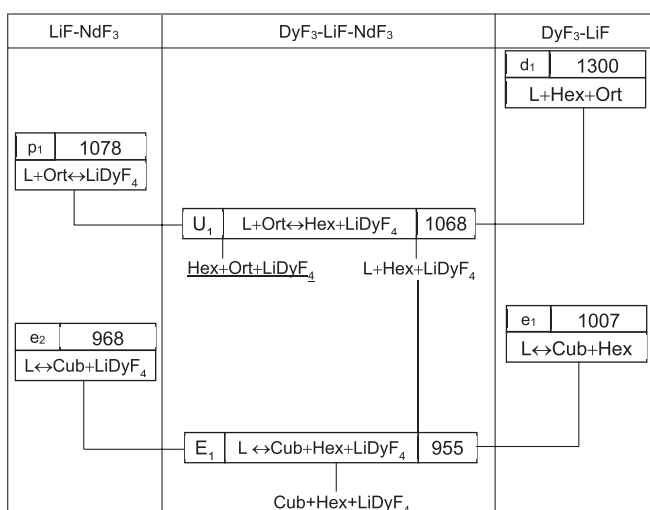


Fig. 7. Reaction scheme for  $\text{DyF}_3\text{-LiF-NdF}_3$  system.

- 045208.
- [22] I.A. dos Santos, D. Klimm, S.L. Baldochi, I.M. Ranieri, Thermodynamic modeling of the LiF-YF<sub>3</sub> phase diagram, *J. Cryst. Growth* 360 (2012) 172–175.
  - [23] R.E. Thoma, G.D. Brunton, Equilibrium dimorphism of the lanthanide trifluorides, *Inorg. Chem.* 5 (11) (1966) 1937–1939.
  - [24] R.J.M. Konings, A. Kovács, Handbook on the physics and chemistry of rare earths, in: Ch. Thermodynamic Properties of the Lanthanide(III) Halides, vol. 33, Elsevier, 2003, pp. 147–247.
  - [25] M. Hillert, B. Jansson, B. Sundman, J. Ågren, A two-sublattice model for molten solutions with different tendency for ionization, *Metall. Trans. A* 16 (1) (1985) 261–266.
  - [26] B. Sundman, Modification of the two-sublattice model for liquids, *Calphad* 15 (2) (1991) 109–119.
  - [27] M. Temkin, Mixtures of fused salts as ionic solutions, *Acta Phys. Chim., USSR* 20 (1945) 411–417.
  - [28] J.-O. Andersson, A. Guillermet, M. Hillert, B. Jansson, B. Sundman, A compound-energy model of ordering in a phase with sites of different coordination numbers, *Acta Metall.* 34 (3) (1986) 437–445.
  - [29] M. Hillert, The compound energy formalism, *J. Alloys Compd.* 320 (2) (2001) 161–176.
  - [30] Grenoble, France, The SGTE (Scientific Group Thermodata Europe) Substance Database, 1997, <http://www.sgte.org>.
  - [31] B. Jansson, Computer Operated Methods for Equilibrium Calculations and Evaluation of Thermodynamic Model Parameters, Ph.D. thesis, Royal Institute of Technology, Stockholm, Sweden, 1984.
  - [32] B. Sundman, B. Jansson, J.-O. Andersson, The thermo-calc databank system, *Calphad* 9 (2) (1985) 153–190.
  - [33] K.C. Hari Kumar, P. Wollants, Some guidelines for thermodynamic optimisation of phase diagrams, *J. Alloys. Compd.* 320 (2) (2001) 189–198.
  - [34] R.E. Thoma, G.D. Brunton, R.A. Penneman, T.K. Keenan, Equilibrium relations and crystal structure of lithium fluorolanthanate phases, *Inorg. Chem.* 9 (5) (1970) 1096–1101.
  - [35] A. Zalkin, D. Templeton, The crystal structures of YF<sub>3</sub> and related compounds, *J. Am. Chem. Soc.* 75 (10) (1953) 2453–2458.
  - [36] F. Spedding, D. Henderson, High-temperature heat contents and related thermodynamic functions of seven trifluorides of the rare earths: Y, La, Pr, Nd, Gd, Ho, and Lu, *J. Chem. Phys.* 54 (6) (1971) 2476–2483.
  - [37] F. Spedding, B. Beaudry, D. Henderson, J. Moorman, High temperature enthalpies and related thermodynamic functions of the trifluorides of Sc, Ce, Sm, Eu, Gd, Tb, Dy, Er, Tm, and Yb, *J. Chem. Phys.* 60 (4) (1974) 1578–1588.
  - [38] B. Sobolev, P. Fedorov, D. Shteynberg, B. Sinitsyn, G. Shakhalamian, On the problem of polymorphism and fusion of lanthanide trifluorides. i. the influence of oxygen on phase transition temperatures, *J. Solid State Chem.* 17 (1) (1976) 191–199.
  - [39] B. Sobolev, P. Fedorov, K. Seiranian, N. Tkachenko, On the problem of polymorphism and fusion of lanthanide trifluorides. ii. interaction of LnF<sub>3</sub> with MF<sub>2</sub> (M = Ca, Sr, Ba), change in structural type in the LnF<sub>3</sub> series, and thermal characteristics, *J. Solid State Chem.* 17 (1) (1976) 201–212.
  - [40] L. Garashina, B. Sobolev, V. Aleksandrov, Y.S. Vishnyakov, On crystallochemistry of rare earth fluorides, *Kristallografiya* 25 (2) (1980) 294–300.
  - [41] S.V. Stankus, R.A. Khairulin, K.M. Lyapunov, Phase transitions and thermal properties of gadolinium trifluoride, *J. Alloys Compd.* 290 (1–2) (1999) 30–33.
  - [42] K. Lyapunov, A. Baginskii, S. Stankus, Experimental study of dysprosium trifluoride enthalpy in solid and liquid states, *J. Thermophys. Aeromech.* 7 (1) (2000) 137–140.
  - [43] J. van der Meer, R. Konings, M. Jacobs, H. Oonk, Thermodynamic modelling of LiF-LnF<sub>3</sub> and LiF-AnF<sub>3</sub> phase diagrams, *J. Nucl. Mater.* 335 (3) (2004) 345–352.